Accepted Manuscript

Mapping groundwater level and aquifer storage variations from InSAR measurements in the Madrid aquifer, Central Spain

Marta Béjar-Pizarro*[1,2,3], Pablo Ezquerro[1,3,5], Gerardo Herrera[1,2,3,4], Roberto Tomás[2,3,6], Carolina Guardiola-Albert[1,7], José M. Ruiz Hernández[8], José A. Fernández Merodo[1,2,3], Miguel Marchamalo[1,3,5], Rubén Martínez[3,5]

* Corresponding author: M.B-P: m.bejar@igme.es

[1] Geohazards InSAR laboratory and Modeling group (InSARlab), Geoscience research department, Geological Survey of Spain (IGME), Alenza 1, 28003 Madrid, Spain.

[2] Research Partnership Unit IGME-UA on radar interferometry applied to ground deformation (UNIRAD), University of Alicante, P.O. Box 99, 03080 Alicante, Spain.

[3] Spanish working group on ground subsidence (SUBTER), UNESCO, Spain.

[4] Earth Observation and Geohazards Expert Group (EOEG), EuroGeoSurveys, the Geological Surveys of Europe, 36-38, Rue Joseph II, 1000 Brussels, Belgium.

[5] Technical University of Madrid. Topography and Geomatics Laboratory. ETSI Caminos, Canales y Puertos, Profesor Aranguren s/n, 28040 Madrid, Spain.

[6] Department of Civil Engineering, University of Alicante, P.O. Box 99, 03080 Alicante, Spain.

[7] Environmental Geology and Geomathematics, Geoscience research department, Geological Survey of Spain (IGME), Alenza 1, 28003 Madrid, Spain.

[8] Hydrogeology and Water quality, Geoscience research department, Geological Survey of Spain (IGME), Ríos Rosas 23, 28003 Madrid, Spain.

Groundwater resources are under stress in many regions of the world and the future water supply for many populations, particularly in the driest places on Earth, is threatened. Future climatic conditions and population growth are expected to intensify the problem. Understanding the factors that control groundwater storage variation is crucial to mitigate its adverse consequences. In this work, we apply satellite-based measurements of ground deformation over the Tertiary detritic aquifer of Madrid (TDAM), Central Spain, to infer the spatio-temporal evolution of water levels and estimate groundwater storage variations. Specifically, we use Persistent Scatterer Interferometry (PSI) data during the period 1992-2010 and piezometric time series on 19 well sites covering the period 1997-2010 to build groundwater level maps and quantify groundwater storage variations. Our results reveal that groundwater storage loss occurred in two different periods, 1992-1999 and 2005-2010 and was mainly concentrated in a region of ~200 km^2. The presence of more compressible materials in that region combined with a long continuous water extraction can explain this volumetric deficit. This study illustrates how the combination of PSI and piezometric data can be used to detect small aquifers affected by groundwater storage loss helping to improve their sustainable management.

1. Introduction

Groundwater is a very precious resource that represents almost 99% of all liquid freshwater on Earth and is a fundamental source for industrial, agricultural and domestic water supply in many regions of the world (Alley et al., 2002; Zektser & Everett, 2004). Groundwater represents the main source of water for many populations and its use increases during drought periods. This contributes to generate a great

stress on aquifer-systems that can lead to a loss of groundwater storage when equilibrium between withdrawals and recharge is unattainable (Döll et al., 2012; Famiglietti, 2014). A recent study using satellite measurements of Earth's gravity shows that a third of big groundwater basins are in distress threatening regional water security and resilience (Richey et al., 2015a). This problem will be exacerbated by climate change and rapid population growth particularly in densely populated areas in arid and semi-arid environments (Döll, 2009; European Union, 2016; Famiglietti, 2014; Ferrant et al., 2014; Taylor, 2014; Wada & Bierkens, 2014). Hence monitoring the evolution of piezometric levels and quantifying groundwater storage variations is essential for identifying vulnerable areas experiencing groundwater storage loss and achieving sustainable water management of aquifers, especially in arid areas prone to droughts.

Estimates of piezometric levels are generally based on networks of wells monitoring water level variations (Fasbender et al., 2008; McGuire et al., 2003). Unfortunately, in many regions around the world, groundwater levels are poorly monitored due to the high cost of piezometers and, thus, information regarding the spatio-temporal evolution of groundwater resources is extremely limited and shows a wide dispersion (Shah et al., 2000).

Groundwater storage can be estimated by combining measurements of changes in groundwater levels over time and area with estimates of storativity (Davis, 1982; McGuire, 2003). These studies are generally based on punctual measurements, leading to a high uncertainty in the estimated groundwater storage (Famiglietti, 2014; Richey et al., 2015b). Recently, studies based on satellite measurements of gravity changes over time have greatly improved the monitoring of groundwater level changes and storage variations (Forootan et al., 2014; Famiglietti et al., 2011; Feng et al., 2013; Jiao, Zhang & Wang 2015; Richey et al., 2015a; Tangdamrongsub et al., 2016; Voss et

al., 2013), helping to identify large areas where groundwater depletion is occurring and quantify the loss of groundwater storage. These studies are very useful to detect large-scale groundwater storage variations, but lack the spatial resolution to characterize and monitor small-scale water loss. Satellite-based methods to measure terrain deformation, specifically Differential Interferometric Synthetic Aperture Radar (DInSAR) and Persistent Scatterer Interferometry (PSI) techniques, have been successfully used to detect and monitor aquifer-related deformation (e.g., Colesanti et al., 2003; Lanari et al. 2004; Schmidt & Burgmann, 2003), estimate aquifer hydraulic properties (e.g., Hoffmann et al., 2001; Tomás et al. 2009; Ezquerro et al., 2014) and model hydraulic head at well locations (e.g., Reeves et al., 2014, Chen et al. 2016). Finally, the potential of InSAR and PSI techniques to predict water level changes at basin scale has been evaluated, with promising results (e.g., Chaussard et al. 2014, Chen et al. 2016, Castellazzi et al. 2016).

The situation of groundwater reserves in Spain, which is the most arid country in Europe, is largely unknown because the number of private extraction wells remains uncertain, and thus the pumped volumes are not known (Hernández-Mora et al. 2007, Llamas & Garrido, 2007; WWF/Adena 2006). The Tertiary detritic aquifer of Madrid (TDAM), in central Spain (Fig. 1) is of strategic importance because it provides water to Madrid, the most populated city of Spain (3.2 million inhabitants in the metropolitan area), during drought periods. Numerical models for the entire aquifer suggest that piezometric levels tend to decline due to groundwater extraction, even when simulated scenarios include recovery periods (Iglesias-Martín et al., 2005; Martínez-Santos et al., 2010). These regional studies could be uncertain since they are based on discrete water level measurements obtained in wells and piezometers. In this study, we reduce this hydrogeological uncertainty taking advantage of the spatial coverage of PSI data to map in detail the evolution of groundwater level and groundwater storage in two extractions areas of the TDAM along several extraction/recovery periods.

4

This paper is organized as follows. In section 2, we give an overview of the Tertiary

detritic aquifer of Madrid, including its main characteristics and deformation behaviour

according to previous studies. In sections 3 and 4, we summarize the PSI and

piezometric data and we describe the methodological approach. In section 5, we show

the main results regarding the stress-strain analyses at 19 wells, the predicted

groundwater levels and the groundwater storage variations. Finally, the potential

factors controlling the observed groundwater loss and the implications of our results for

the management of water extractions during future droughts in the TDAM are

discussed.

FIGURE 1 LOCATION

2. The Tertiary detritic aquifer of Madrid

The TDAM is located in the northwest part of the Madrid basin (Fig. 1a), a tectonically

controlled, triangular shape basin of ~6000 km^2 area, which is filled with materials

deposited in continental environments from Late Cretaceous to Upper Miocene (IGME

2000). The detritic facies of these deposits define the TDAM. The basin is bounded by

the Toledo Mountains to the south, the Altomira Range to the southeast and the

Central System Range to the northwest. The region is crossed by several large rivers

such as the Guadarrama, the Manzanares and the Jarama rivers (Fig. 1a).

The TDAM is a heterogeneous and anisotropic aquifer system with elevation between

650 to 800 meters above sea level (Hernández-García & Custodio, 2004; Yélamos &

Villarroya, 2007; Martínez-Santos et al., 2010). The aquifer system, with a thickness of

more than 3 km and a multilayer structure, is formed by a series of metric sand lenses

embedded in a low-permeability clay matrix. The coarse fraction mainly consists of

arkosic sand and the fine fraction is a mixture of smectite, illite and a low percentage of

5

kaolinite (IGME, 2000; IGME, 1989). Those deposits are the result of the erosion of the mountain range to the northwest and show a spatially variable percentage of the fine fraction along the study area (Fig. 1c), with a clear increasing trend from northeast (25%) to southwest (68%). Total groundwater stored in the TDAM is at least 20,000 Million Cubic Meters (MCM) (Llamas, Villarroya & Hernández-García, 1996).

A network of 70 wells created in 1970, with a capacity between 60 and 80 MCM/year, provides water to the city during drought periods. In this study we focus on two extraction areas located in the north-northwest of Madrid City, herein referred to as the northern and southern extraction fields that cover an area of 500 km^2 (Fig. 1b). Groundwater extraction wells in these areas (white dots in Fig. 1a,b) present average depths between 300 and 700 m below the ground surface, which has an average elevation of ~700 m above sea level in these areas (Fig. 1a). From 1991 to 2011, these well fields experienced five cycles of groundwater extraction and recovery, coinciding with two drought periods: the 1991-1995 and 2004-2006 droughts (Ministerio de Medio Ambiente, 2007). In the southern extraction field there are also numerous shallower wells less than 300 m depth, which are mainly exploited by private individuals.

Land deformation associated to groundwater level changes in the TDAM has been reported in previous works. Ezquerro et al. (2014) combined PSI-derived deformation time series (from ERS and ENVISAT data) with piezometric data from 18 wells to characterize the deformational behaviour of the TDAM. These authors concluded that the aquifer system behaves almost elastically through cycles of groundwater pumping and recovery, and ground uplift during recovery periods almost cancels out the land subsidence measured during previous extraction periods. Using the same PSI and piezometric dataset plus piezometric time series from one additional well, Béjar-Pizarro et al. (2015) evaluated the potential of PSI data to infer the spatio-temporal evolution of piezometric levels in the TDAM and concluded that the relationship between ground

6

deformation and water level was very stable among the wells sites and could be

modelled using an average S_{ke} of all wells. In this study, we use the same dataset that

Béjar-Pizarro et al. (2015) to go beyond previous studies by 1) modelling groundwater

levels over the entire extraction fields and 2) mapping groundwater storage changes to

identify regions affected by storage loss.

3. Data

3.1 PSI data

PSI data used in this work are from Ezquerro et al. (2014). They consist of 50 ERS

satellite SAR images in a descending track mode between 1992 and 2000 and 31

ENVISAT satellite SAR images in an ascending track mode acquired between 2003

and 2010. Using the PSP-IFSAR technique (Costantini et al. 2008) the deformation

time series in the satellite line-of-sight direction were estimated for each Persistent

Scatterer (PS). Deformation time series estimated from ERS data are relative to date

19/04/1992 and deformation measurements from ENVISAT data are relative to date

05/08/2003. See Ezquerro et al. (2014) for more details about the PSI processing.

PSI-derived maps show deformation concentrated around the extraction fields, with

most of the deformation distributed within a 6-km radius from the wells (Fig. 2). In the

central region of the deformation maps there is a lack of PSI data due to the presence

of a densely vegetated area, which produces the loss of signal by decorrelation.

Ground displacement ranges between 8.4 cm (movement away from the satellite)

during extraction period 5 (26 April 2005 - 3 October 2006) and 8.44 cm (movement

towards the satellite) during recovery period 5 (3 October 2006 - 7 September 2010).

PSI deformation measurements are in the satellite line-of-sight direction, which is 23º

from the vertical. Since we only have one acquisition mode (ascending or descending)

for each dataset, we could not estimate horizontal and vertical components of the

deformation field. We assume that the main contribution to the displacement field is from vertical deformation, which is reasonable considering that the velocity gradient measured in the border of the subsiding area is low (~7 mm/yr over 2 km) and thus we do not expect to have significant horizontal deformation.

Figures 2c and 2d shows deformation time series (black lines) over well FE-1R, located in the northern extraction field, and over well MJ-1, located in the southern extraction field. We observe ground subsidence followed by uplift during the consecutive periods of water extraction and recovery. Note that there is a discontinuity in the deformation time series between ERS and ENVISAT periods (represented by two grey horizontal bars in Fig. 2 c,d) and thus the period 2000 to 2003 is not covered by PSI data.

FIGURE 2 LOCATION

3.2 Piezometric data

The piezometric data consist of groundwater level time series with monthly sampling at 19 well sites covering the period 1997-2010. 18 wells are located in the northern extraction field (Ezquerro et al., 2014) and only well MJ-1 is located in the southern extraction field (Fig. 1b). Figure 2 c,d shows piezometric time series for wells FE-1R and MJ-1, respectively (blue lines). Piezometric data cover three complete cycles of groundwater extraction and recovery, which are delimited by the vertical dashed lines in Figure 2 c,d. Groundwater level changes of more than 100 m are observed during some extractions periods (e.g. extraction 5 in well FE-1R, Fig. 2c)

4. Methodology

4.1 Estimation of the elastic coefficient of storage (S_{ke})

Recharge and withdrawal of groundwater in a confined aquifer produce changes in the

thickness of the aquifer that are directly related to ground deformation. The deformation of the aquifer-system can be inelastic (partially recoverable) or elastic (totally recoverable) depending on whether or not the applied stresses are beyond its previous maximum level (preconsolidation stress threshold). To investigate how the TDAM behaves during the period 1997-2010 we studied the relationship between ground deformation and groundwater level evolution on 19 well sites (Fig. 1b). Using the graphical methodology proposed by Riley (1969), we determined the stress-strain relationship at well locations comparing water levels and PSI-derived ground displacements. Since deformation data are separated in two temporal periods (ERS and ENVISAT periods), we analyse the stress-strain trajectories independently for the two periods. To obtain the elastic coefficient of storage due to expansion and compression of the matrix of the aquifer system S_{ke}, we estimate the inverse slope of the stress-displacement data trend line (Riley, 1969; Riley, 1984). For each well site, we analyse independently each period and then we estimate the average value. Note that this analysis is different to that performed by Ezquerro et al. (2014), that only considered the 1997-2000 period, and to the study of Béjar-Pizarro et al. (2015), that analysed jointly the two periods. Here we estimate the S_{ke} by analysing separately the stress-strain trajectories for each period, in order to evaluate the stability of the S_{ke} value and detect changes in the behaviour of the aquifer.

4.2 PSI based groundwater level maps

First maps of relative groundwater level were created: for that, deformation maps for each SAR date were converted to groundwater level maps by applying the average S_{ke} to each PSI observation. To transform them into piezometric maps relative groundwater level must be combined with a reference piezometric map. The reference piezometric map was built compiling all the available groundwater measurements in extraction wells and piezometers in the region for the date May 1st 2008. We considerer that piezometric levels remained unchanged betwen the date of this reference map

9

and the closest SAR date (July 29th 2008). This assumption is based on the fact that

there are only three months between the two datasets used for the map generation and

they are located within a period of stability in the aquifer. Note that using this map as a

reference, only piezometric maps for the ENVISAT period (2003-2011) can be

produced, since the gap between ERS and ENVISAT data (2000-2003) does not allow

to reference groundwater level maps during the ERS period (1992 – 2000).

To produce continuous piezometric maps, groundwater level estimations in regions

without PSI data were interpolated using geostatistical techniques (see section 4.3).

Groundwater maps were previously resampled to reduce the high density of data (10^5

in a 40x40 km region) to ~ 5000 points.

The analysis has been carried out only within a 6-km distance from the wells. This

distance corresponds to the influence area of ground deformation around the well fields

deduced by Ezquerro et al. (2014) and the extent of pumping effects around the

northern extraction field observed by Yélamos & Villarroya (1991).

4.3 Interpolation of groundwater level maps

To interpolate groundwater level estimations in regions where PSI data could not be

retrieved due to decorrelation, we use the ordinary kriging method (Isaaks &

Srivastava, 1989). Kriging has been recommended as the best method to interpolate

point data since it minimizes the error variance using a weighted linear combination of

the data (Goovaerts, 1997). This geostatistical tool is based on the variogram function

to characterize the spatial variation of the variable to be interpolated. The analysis was

carried out with the Stanford Geostatistical Modeling Software (SGeMS) package

(Remy, Boucher & Wu, 2009).

The original high density groundwater level maps were subsampled to 5000 points to

compute the directional variograms and identify potential anisotropy in the data. The

modelled variogram was used to interpolate each groundwater level map.

4.4 Groundwater storage variation (ΔV)

Groundwater volumetric changes for a period can be estimated by subtracting the groundwater surfaces at the beginning and end of the period. This can be used in conjunction with the coefficient of storage or Storativity (S) to obtain the groundwater storage variation *(ΔV)*, i.e. the difference between aquifer-system storage at the beginning and end of the studied period. In a confined aquifer, *(ΔV)* can be estimated as (Davis, 1982):

$$\Delta V = A \times \Delta H \times S = A \times \Delta H \times S_S \times b \qquad (1)$$

where A is the surface area of the aquifer-system (m^2); ΔH is the difference between the water levels (m), b is the aquifer thickness (m) and S_s is the aquifer-system specific storage (m^{-1}).

To estimate groundwater storage variations in the aquifer, the value of the aquifer coefficient of storage (S) was first calculated. S is defined as the volume of water released per unit area from a layer of thickness b due to a unit decline in the piezometric surface (Todd, 1980).

In a confined aquifer-system, water is derived both from reduction of pore space (resulting in compaction of the system) and expansion of the pore water as the pore pressure declines. The aquifer-system coefficient of storage S includes the two terms, the compressibility of the matrix of the aquifer-system and the water compressibility:

$$S = S_S \times b = \left(\beta_p + n \times \beta_w\right) \times \rho_w \times g \times b = \ (S_{sk} + S_{sw}) \times b = S_k + S_{sw} \times b$$

$$(2)$$

where $_p$ is the oedometric compressibility of the matrix (m^2/N); $_w$ is the volumetric compressibility of water (4.8 x 10^{-10} m^2/N); $_w$ is the water density (1000 Kg/m^3); g is the acceleration of gravity on the surface of Earth (9.81 m/s^2); n is the porosity of the aquifer, and ranges from 1% to 20% (Rodríguez, 2000); S_{sw} is the specific storage due to expansion or contraction of the water (m^{-1}) and S_{sk} is the specific storage due to expansion or contraction of the matrix (m^{-1}). The different deformation behaviour of the

11

soil to stress induced by the hydraulic head variations is described using two different specific storage due to matrix, inelastic, S_{skv}, and elastic, S_{ske} (Galloway, 1998; Sneed & Galloway, 2000).

Finally, **ΔV** was estimated during each cycle of groundwater extraction and recovery using the estimated coefficient of storage S and the groundwater level maps corresponding to the dates limiting each cycle, considering both, ERS and ENVISAT periods, by means of eq. (1).

5. Results

5.1 Stress-strain analyses

Figure 3 shows the stress-strain relationship at 4 well locations. Groundwater level variations represent the induced stresses and the ground displacements represent the vertical deformation of the aquifer system. The hysteresis loops obtained for all the wells represent the elastic stress/strain behaviour resulting from groundwater level variations that do not drop below the preconsolidation stress threshold (Riley, 1984; Sneed & Galloway, 2000). These trajectories, characteristic of elastic and recoverable deformation (Riley, 1984), indicate that during the period 1997-2010 the TDAM behaves elastically. Note that during the period 1992-1997 only deformation data are available and thus the stress-strain analysis cannot be performed (Figs. 2 c,d). Therefore, the elastic behaviour of the TDAM deduced from our stress-strain analysis is only observed during the 1997-2010 period.

FIGURE 3 LOCATION

The stress-strain trajectories for each period are very similar in most of the wells (Fig. 3 and Appendix A). The S_{ke} values of each well site, obtained by averaging the slope of the trend line for the ERS and ENVISAT period (grey and black trajectories in Figure 3)

12

are shown in Table 1. For the northern extraction field, S_{ke} values vary from 2.29 x 10^{-4} at well CB-5 to 6.84 x 10^{-4} at well CB-15 (Table 1). The only well site at the southern extraction field where S_{ke} could be estimated, MJ-1 (Fig. 1b) presented a S_{ke} of 4.02 x 10^{-4}, which is also within the range of S_{ke} values in the northern extraction field, suggesting that there is not a significant difference between both well fields in terms of the S_{ke} value. Retrieved values are very similar to those estimated by Béjar-Pizarro et al. (2015) analysing the same time interval, and by Ezquerro et al. (2014) for a shorter time interval. This suggests that the S_{ke} values are quite stable and independent of the considered time interval, provided that the aquifer-system is not stressed beyond its preconsolidation stress threshold.

Table 1 | Elastic storage coefficient (S_{ke}) estimated for the 19 well sites in this study. The root mean square (rms) and average difference between modelled and observed hydraulic head at each well location are shown for two groups of models: 1) Hydraulic heads estimated using the S_{ke} of each well and 2) Hydraulic heads estimated using the average S_{ke} (computed from all 19 wells labelled in Fig. 1b). Percentage errors are estimated by comparing average errors with the maximum measured groundwater level variations for every well. Observed and modelled hydraulic heads are shown in Fig. 4.

Well Name	S_{ke}	Models using well S_{ke}			Models using average S_{ke}		
		rms	Average error (m)	Percentage error (%)	rms	Average error (m)	Percentage error (%)
CA-3	4.02E-04	29.5	19.7	12	30.4	19.8	12
CA-4	3.62E-04	25.3	18.6	13	27.2	18.7	14
CA-5	3.47E-04	21.9	16.6	11	25.0	18.5	13
CB-4	3.56E-04	33.8	24.7	15	36.2	24.8	16
CB-5	2.29E-04	41.6	32.6	18	52.1	36.1	19
CB-6	2.87E-04	51.1	31.9	16	56.6	30.3	15
CB-9	3.00E-04	46.8	37.4	22	53.1	41.7	24
CB-11	3.42E-04	21.8	15.8	11	26.4	19.1	13
CB-12	4.67E-04	20.9	14.5	11	20.8	15.6	11
CB-13	4.52E-04	20.7	15.5	12	20.6	15.7	12
CB-14	4.27E-04	21.6	14.9	12	21.6	14.9	12
CB-15	6.84E-04	19.3	15.4	12	37.2	29.7	23
FA-1	5.89E-04	27.3	18.3	16	30.2	23.0	20
FA-3	5.14E-04	22.8	16.8	12	23.1	16.7	11
FC-2	5.09E-04	36.7	33.3	25	44.8	40.4	30
FX-4	5.27E-04	24.5	18.4	13	26.7	21.7	15
G-I	3.15E-04	26.3	19.7	12	33.6	24.1	15
FE-1R	5.04E-04	18.3	13.4	10	20.8	14.3	10

MJ-1	4.02E-04	29.3	24.6	21	28.1	23.3	20
Average	4.22E-04	28.4	21.2	14	32.3	23.6	16

5.2 Groundwater level estimation

The obtained S_{ke} values were used to predict groundwater levels at specific well

locations during the SAR acquisitions time period and compared against measured

groundwater levels. The observed and modelled groundwater levels show a good

match, with the Pearson correlation coefficients varying between 0.65 and 0.92. To

evaluate the effect of using a constant S_{ke} value for the entire study region, models

were elaborated using also the average S_{ke} value for all wells (4.22×10^{-4}). The

comparison of estimated and measured groundwater levels at different wells is shown

in Figure 4. The average error between observations and these models, estimated as a

percentage of the total water level change during the study period (Ezquerro et al.

2014), is very similar: 14% for models using the S_{ke} of each well and 16% for models

using the average S_{ke} for all wells (Table 1). This result suggests that an average S_{ke}

can be used to estimate piezometric level variations in all the points where ground

deformation has been measured by PSI, permitting the elaboration of piezometric level

maps for the different extraction/recovery cycles.

FIGURE 4 LOCATION

Groundwater levels were estimated in all the PSI data points by applying the average

S_{ke} to each PSI observation. After applying the ordinary kriging method to interpolate

groundwater level values in the regions not covered by PSI data (Appendix B) maps of

relative groundwater level were obtained for each SAR date.

Figure 5 shows the contours of groundwater level in the TDAM obtained for the dates

that limit the different cycles of groundwater extraction and recovery within the 2003-

14

2011 period. The reference piezometric map is also shown (Fig. 5d). This map indicates that groundwater system recharge comes from watersheds precipitation. This is not in contradiction with the behaviour of the deep confined aquifer system: infiltration in recharge areas reaches the water table through a thick unsaturated zone with low vertical permeability (Martínez-Santos et al., 2010). From these areas water flows into the valleys where the aquifer discharges along the rivers and the quaternary alluvial. All maps show minimum groundwater levels around both wells fields, which clearly control the groundwater level in the aquifer during the study period. To the south of the southern extraction field there is a region of higher piezometric levels which is already present in the reference piezometric map (Fig 5d) and can be attributed to the lack of pumping wells in that region.

FIGURE 5 LOCATION

Water levels vary between 400 and 700 m a.s.l, with lower levels located in the map dated October 3rd 2006 (Fig. 5c), which corresponds to the end of the extraction phase 5 and coincides with the end of the severe drought that affected Spain in 2006. The higher levels of groundwater are registered in the map of November 1st 2005 (Fig. 5b), which corresponds to the end of recovery period 4.

Piezometric maps were validated with hydraulic heads measured at the 19 well sites (Table 2). The average error among the 19 well sites varies between 2.5 m (2% error) in the May 1st 2008 map and 28.7 m (20% error) in the September 7th 2010 map.

Table 2 | Average error (in m) between observed and modelled groundwater level at each well location for the groundwater contour maps in Fig. 5. Percentage errors estimated by comparing average errors with the maximum measured groundwater level variations for every well are also shown.

15

Dates	20030805		20050111		20061003		20080501		20100907	
Well	Err (m)	Err (%)	Err (m)	Err (%)	Err (m)	Err (%)	Err (m)	Err (%)	Err (m)	Err (%)
CA-3	-7.9	5	19.3	12	-1.9	1	-1.9	1	25.4	15
CA-4	-2.8	2	27.5	19	17.6	12	-3	2	34.9	24
CA-5	-5.4	4	25.4	17	28.4	19	0.8	1	35.4	24
CB-4	-26.9	16	20.3	12	3.9	2	1	1	31	19
CB-5	15.9	9	23.1	12	92.1	49	-1	1	24.9	13
CB-6	15.2	7	29.3	14	23.9	11	1.7	1	14.7	7
CB-9	-17.6	10	23	13	4.4	3	-2.8	2	32.1	19
CB-11	-1.4	1	21.4	15	18.3	13	4.1	3	37.5	26
CB-12	-16.2	11	20.2	14	-13	9	-0.7	1	11.7	8
CB-13	-13.8	10	6.7	5	-15.6	12	-6.2	5	4.9	4
CB-14	-8.1	6	26.4	21	-9.9	8	2.6	2	5.3	4
CB-15	0	0	25.6	19	-14.3	11	1.1	1	9.7	7
FA-1	-17.7	15	28.7	24	-25	21	-0.1	0	55.8	46
FA-3	-14.3	10	6.9	5	1.8	1	-2	1	47.3	32
FC-2	-21.1	16	8.1	6	-9.4	7	-1.9	1	31.2	23
FX-4	-3.9	3	30.5	20	5.4	3	0.8	1	40.9	26
G-I	0.7	0	27.5	17	51.7	31	5	3	36.7	22
FE-1R	-3.9	3	23.2	16	13.6	10	1.1	1	40.3	29
MJ-1	16.1	13	30.7	25	21.6	18	10.3	9	26	22
Av_Error	11	7	22.3	15	19.6	13	2.5	2	28.7	20

5.3 Groundwater storage variation (ΔV)

We estimated ΔV by using the estimated groundwater level maps and equation (1).

First, the aquifer coefficient of storage (S) was estimated using equation (2). In the

case of the TDAM, where aquifer-system layers are mainly composed of coarse-

grained deposits and exhibit a clear elastic behaviour, the inelastic component is

assumed to be negligible for the period 1997-2010 and then $S_{sk} = S_{ske}$ and $S_k = S_{ke}$.

A value of 154 m was estimated for the aquifer thickness (b) by averaging the

thickness of aquifer layers in the well sites where lithological data were available. The

aquifer-system storage coefficient S was calculated using the average S_{ke} and the S_{sw}

values obtained for three different porosity values (Rodriguez, 2000), resulting in 4.29 x

10^{-4}, 4.92 x 10^{-4} and 5.63 x 10^{-4} for 1%,10% and 20% porosity, respectively. These

values are consistent with coefficients of storage derived from pumping tests, that

range between 10^{-3} and 10^{-4} (Canal de Isabel II Gestion, 2014).

Then, ΔV was estimated during each period of water extraction and recovery using the groundwater level maps corresponding to the dates that limit each cycle, considering both, ERS and ENVISAT periods. Based on the stress-strain analysis for the period 1997-2010 we assume an elastic behaviour of the aquifer system to estimate ΔV changes along the complete period cover by PSI data, including the 1992-1997 interval. Note that we could not characterize the elastic/inelastic behaviour of the aquifer system during this period because piezometric data were not available until 1997. In this period, a greater nonrecoverable deformation seemed to affect the TDAM (Ezquerro et al. 2014) and thus the assumption of an elastic behaviour could be incorrect. Considering that deformation during 1992-1997 could be dominated by the inelastic component of deformation, and taking into account that the inelastic coefficient of storage is always higher than the elastic coefficient of storage (Ireland et al. 1984), groundwater storage estimations for the 1992-1997 period represent a maximum value. In fact, note that for a given deformation, the groundwater level drop necessary to trigger it will be higher if there is an elastic response than an inelastic one.

Table 3 shows the volumetric changes in the groundwater for each extraction/ recovery cycle using three values of porosity (1%, 10% and 20%). The groundwater storage between consecutive cycles completely covered by our PSI data (i.e. Ext1-Rec1, Ext2-Rec2 and Ext5-Rec5, Fig. 2 c,d) was compared to evaluate if groundwater variations are compensated at the end of each extraction/recovery cycle. The difference is negative in all cases, indicating that groundwater depletion during extraction cycles is not completely compensated during the recovery phase causing a groundwater storage loss after each cycle.

Table 3 | Groundwater storage variation in Million Cubic Meters (MCM) estimated for each extraction / recovery cycle in the area shown in Fig. 6 (545 km^2). * indicates maximum value. Negative differences between consecutive extraction / recovery phases indicate a groundwater loss during the complete cycle. Question marks indicate that groundwater variation within the cycle could not be estimated because the cycle was not completely covered by PSI data. Volumes have been estimated using three porosity values (1%, 10% and 20% porosity).

	cycle	Ext1	Rec1	Ext2	Rec2	Ext3	Rec3	Rec4	Ext5	Rec5
porosity 1%	volume (MCM)	-6.8*	0.6*	-6.8*	5.5*	-11.4	1.6	6.9	-17.0	12.8
	difference (MCM)	-6.3*		-1.3*		?		?	-4.2	
porosity 10%	volume (MCM)	-7.8*	0.6*	-7.8*	6.3*	-13.1	1.8	8.0	-19.5	14.6
	difference (MCM)	-7.2*		-1.5*		?		?	-4.8	
porosity 20%	volume (MCM)	-9.0*	0.7*	-8.9*	7.2*	-15.0	2.1	9.1	-22.3	16.7
	difference (MCM)	-8.2*		-1.8*		?		?	-5.5	

FIGURE 6 LOCATION

Maps of groundwater storage variation permit to visually identify regions where the loss and recovery of groundwater occurs in each period. Figures 6a and 6b depict maps of groundwater storage variation for extraction period 5 and recovery period 5. The greatest volume variation occurs around the extraction fields, with a similar pattern but different magnitude in each period. To detect regions with groundwater storage loss, we compare groundwater storage maps corresponding to the beginning of water extraction with maps corresponding to the end of recovery. We consider the longest time interval covered by PSI data and spanning complete consecutive cycles of water extraction and recovery. Cycles not completely covered by PSI data (i.e. Ext3, Rec3, Ext4 and Rec4) are not taken into account. For the ERS period, we estimate the groundwater storage difference between the beginning of extraction period 1 and the end of recovery period 2 (Fig 7a). The groundwater deficit volume is concentrated in the southern extraction field, except for some isolated patches of deficit volume in the

northern extraction field (in a region not well covered by PSI data and out of the well

sites location). For the ENVISAT period, we estimate the groundwater storage different

between the beginning and the end of cycle 5, which is the only complete cycle (Figure

7c). The groundwater storage difference is also mainly concentrated in the southern

extraction field.

FIGURE 7 LOCATION

 The average groundwater storage loss in Figures 7a and 7c is 8.8±1.2MCM and

4.9±0.7MCM respectively, which is estimated considering the different values of

porosity (Table 3). Since we have established a direct relationship between ground

deformation and groundwater level, areas with cumulated subsidence represent areas

where extracted groundwater is not compensated by recharge during recovery periods

and thus are prone to suffer a storage loss of the aquifer. Fig. 7b corresponds to

differential deformation between April 19th 1992 and January 27th 1999 and Fig. 7d

shows the differential deformation between January 11th 2005 to September 7th 2010.

While the region of the southern extraction field shows a clear cumulated deformation,

it seems to be compensated in the northern extraction field during consecutive cycles.

Comparing these maps of cumulated subsidence with maps of groundwater storage

deficit for the same period (Fig 7a,c) the same features can be identified in the

southern extraction field. Contrarily, in the northern extraction field, the groundwater

storage deficit areas (indicated by letters a,b,c in Fig. 7 a,c) do not correspond to

deformation areas and can only be explained as artefacts from the interpolation. These

patterns can also be observed in the deformation time series. In the northern extraction

field (well site FE-1R) both water level and ground elevation seem to return to their

original position at the end of recovery periods 2 and 5 (Fig. 2c), whereas in the

southern extraction field (well site MJ-1) ground does not recover its original elevation

at the end of these recovery periods (Fig. 2d).

19

6. Discussion and conclusions

In this study we have used 15 years of deformation data over the TDAM to provide spatially continuous measurements of groundwater level and groundwater storage in two extractions areas of the aquifer, along several extraction/recovery periods.

Based on our analysis of the stress-strain diagrams on 19 well sites for the period 1997-2010 we assume an elastic behaviour for the aquifer system. Ground uplift during recovery periods compensates most of the ground subsidence measured during previous extraction. However, a nonrecoverable component of the deformation is observed, especially in the southern extraction field (e.g. deformation time series for well site MJ-1 in Fig. 2d). This inelastic response was more intense during the period 1992-1997 (for which piezometric data are not available) and is probably responsible for the groundwater storage deficit measured in this area. In this period, estimations of groundwater storage variations assume an elastic behaviour and represent a maximum value.

The variation of groundwater storage during the extraction periods ranges between 6.8 MCM and 17 MCM (8.9 and 9.8 MCM/yr), respectively, and represent 22-31% of the maximum annual extraction capacity of these well fields (Canal de Isabel II Gestión, 2014). The comparison of volumetric changes in the groundwater during consecutive extraction/recovery cycles reveals a negative volumetric difference in all cases (Table 3), indicating a smooth piezometric declining trend. This deficit occurred during two different periods, 19/APR/1992-27/JAN/1999 and 11/JAN/2005-07/SEP/2010, coinciding with two severe droughts and is mainly concentrated in an area of ~200 km^2 in the southern extraction field (Fig. 7). This region has experienced a high urbanization rate in the last decades (Fig. 1c) and is characterized by the existence of

20

multiple private wells exploited by local entities and individuals for water supply, with scarce public planning or control (WWF/Adena, 2006). While wells for urban supply only operate during drought periods, private wells are extracting groundwater continuously due to its lower price (Llamas, 2007). The TDAM in the southern extraction field area includes a greater percentage of low-permeability materials compared to the northern field (Fig. 1c). The combination of these two factors, a sustained groundwater extraction, which is more intense during drought periods, and the presence of more compressible materials in the aquifer, could explain the capacity loss of the reservoir. Preventing the continuation of this tendency in the southern extraction during future droughts probably requires the interruption or reduction of groundwater pumping during some periods so that groundwater levels can recover.

One of the main sources of uncertainty of the estimated groundwater storage variations comes from the incertitude of the aquifer parameters, such as porosity and thickness of aquifer layers that have been taken as an average value. Our results can be updated when more precise measurements of the aquifer parameters will be available and this would impact the estimated groundwater volumes. These parameters, although necessary to quantify the volumetric deficit, are not needed to detect the areas with groundwater storage loss, whose detection depends exclusively on the PSI-derived deformation (e.g. Figure 7). Other uncertainty source of the estimated groundwater storage variations comes from the loss of coherence in the PSI data. Groundwater data have been interpolated in areas affected by decorrelation and, consequently, groundwater level estimations are less reliable in these regions. The uncertainty in the deformation time series results depends on multiple factors regarding the SAR dataset, the PSI processing and the characteristics of the targeted deformation (Crosetto et al., 2015; Hanssen, 2001), However, the errors in our PSI data do not seem significant in view of the striking similarity between deformation and observed groundwater levels (Fig. 2 c,d). Considering that the average groundwater level variations for the 19 wells

over the study period is 146 m and the average root mean square error between real and modelled groundwater levels is ~30 m (Table 1), a 80% of the true groundwater level variation is recovered by PSI data.

Due to the limited temporal interval covered by our PSI dataset, the transient or permanent nature of the deformation that remains at the end of recovery periods 2 and 5 (and thus the groundwater storage deficit) is unknown. The possibility that the groundwater storage loss is recovered after the periods used in the study cannot be discarded with our data and thus it should be considered as potentially permanent.

This approach can be applied to other aquifers exhibiting an elastic behaviour. In our case, due to the elastic deformational behaviour of the TDAM during the period 1997-2010, we can assume a unique S_{ke} value that seems to reproduce quite well the observed evolution of groundwater level. In other aquifer-systems where this assumption cannot be used (Amelung et al., 1999; Boni et al., 2015; Calderhead et al., 2011) the approach is still valid, but a spatially variable coefficient of storage also including the inelastic compressibility of the aquifer-system skeleton should be considered instead (Galloway et al. 1998).

There is growing evidence that groundwater resources are decreasing in many regions of the world (Famiglietti, 2014; Feng et al., 2013; Shah et al. 2000; Wada & Bierkens; 2014). While GRACE data are helping identifying big groundwater bodies under stress (Richey et al., 2015a), this study illustrates how PSI data can complementary be applied to a more local scale to detect groundwater storage loss of small aquifers helping to improve their sustainable management in future droughts. The historical archive of SAR data suitable for InSAR, acquired since the early 1990s by different satellites (Hooper et al., 2012), along with the new Sentinel-1 satellites, with a global

22

coverage and 6 days revisit time, guarantee the availability of InSAR data for virtually studying every aquifer on Earth.

References

Alley, W. M., Healy, R. W., LaBaugh, J. W. & Reilly, T. E. (2002). Flow and storage in groundwater systems. *Science* **296,** 1985–1990; DOI:10.1126/science.1067123

Amelung, F., Galloway, D. L., Bell, J. W., Zebker, H. A. & Laczniak, R. J. (1999). Sensing the ups and downs of Las Vegas: InSAR reveals structural control of land subsidence and aquifer-system deformation, *Geology* **27,** 483-486

Béjar-Pizarro. *et al.* (2015). Evaluation of the potential of InSAR time series to study the spatio-temporal evolution of piezometric levels in the Madrid aquifer. *Proc. IAHS*, **372**,29-32

Boni, R. *et al.* (2015). Twenty-year advanced DInSAR analysis of severe land subsidence: the Alto Guadalentín Basin (Spain) case study, *Eng. Geol.* DOI: 10.1016/j.enggeo.2015.08.014

Calderhead, A. I., Therrien, R., Rivera, A., Martel, R. & Garfias, J. (2011). Simulating pumping induced regional land subsidence with the use of InSAR and field data in the Toluca Valley, Mexico, *Adv. Water Resour.* **34,** 83-97

Canal de Isabel II Gestión. (2014). Captación de aguas de superficie y subterraneas. *Technical report.* (in Spanish). Available at: https://www.canalgestion.es/es/galeria_ficheros/gestionamos/ciclo/Folleto_Captaci xn_2014.pdf (Date of access: 21st March 2016)

Castellazzi, P., R. Martel, A. Rivera, J. Huang, P. Goran, A.I. Calderhead, E. Chaussard, J. Garfias, & J. Salas. (2016). Groundwater depletion in Central Mexico: Use of GRACE and InSAR to support water resources management. *Water Resources Research* **52**. DOI:10.1002/2015WR018211.

Colesanti, C., Ferretti, A., Novali, F., Prati, C. & Rocca, F. (2003). SAR monitoring of progressive and seasonal ground deformation using the permanent scatterers technique. *IEEE Trans Geosci Remote Sens* **4,** 1685–1701.

Costantini, M., Falco, S., Malvarosa, F. & Minati, F (2008). A new method for identification and analysis of persistent scatterers in series of SAR images. Int. Geosci. Remote Sensing Symp. (IGARSS), 449–452.

Crosetto, M., Monserrat, O., Cuevas-González, M., Devanthéry, N. & Crippa, B. (2015). Persistent Scatterer Interferometry: A review. *ISPRS J. Photogramm. Remote Sens.* doi:10.1016/j.isprsjprs.2015.10.011.

Chaussard, E., R. Burgmann, M. Shirzaei, E. J. Fielding, & B. Baker (2014). Predictability of hydraulic head changes and characterization of aquifer-system and fault properties from InSAR-derived ground deformation, *J. Geophys. Res. Solid Earth,* 119, 6572–6590, doi:10.1002/2014JB011266.

Chen, J., Knight, R., Zebker, H.A. & Schreuder, W.A. (2016). Confined aquifer head measurements and storage properties in the San Luis Valley, Colorado, from spaceborne InSAR observations, *Water Resources Research,* 10.1002/2015WR018466.

Davis, G.H. (1982). Prospect risk analysis applied to ground-water reservoir evaluation. *Ground Water* **20,** 657-662

Döll, P. (2009). Vulnerability to the impact of climate change on renewable groundwater resources: a global-scale assessment. *Environ. Res. Lett.* **4**; DOI:10.1088/1748-9326/4/3/035006

Döll, P. *et al.* (2012). Impact of water withdrawals from groundwater and surface water on continental water storage variations*, J. Geodyn.* **59-60,**143-156 (2012).

European Union. Science for Water. *European Commission Joint Research Centre (JRC) thematic report* . Available at:

https://ec.europa.eu/jrc/en/publication/thematic-reports/science-water (Date of access: 21st March 2016).

Ezquerro, P. *et al.* (2014). A quasi-elastic aquifer deformational behavior: Madrid aquifer case study. *J. Hydrol.* **519,** 1192–1204; DOI:10.1016/j.jhydrol.2014.08.040

Famiglietti, J.S. *et al.* (2011). M. Satellites measure recent rates of groundwater depletion in California's Central Valley. *Geophys. Res. Lett.* **38,** L03403.; DOI:10.1029/2010GL046442

Famiglietti, J. S. (2014). The global groundwater crisis. *Nature Clim. Change* **4,** 945–948; DOI:10.1038/nclimate2425

Fasbender, D., Peeters, L., Bogaert, P. & Dassargues, A. (2008). Bayesian data fusion applied to water table spatial mapping. *Water Resour. Res.* **44**, W12422; DOI:10.1029/2008WR006921

Feng, W. *et al.* (2013). Evaluation of groundwater depletion in North China using the Gravity Recovery and Climate Experiment (GRACE) data and ground-based measurements. *Wat. Resour. Res.* **49,** 2110–2118

Ferrant, S. *et al.* (2014). Projected impacts of climate change on farmers' extraction of groundwater from crystalline aquifers in South India. *Sci. Rep.* **4,** 3697; DOI: 10.1038/srep03697.

Forootan, E., Rietbroek, R., Kusche, J., Sharifi, M.A., Awange, J.L, Schmidt, M. , Omondi, P. , Famiglietti, J. (2014). Separation of large scale water storage patterns over Iran using GRACE, altimetry and hydrological data. Remote Sensing of Environment, 140, 580-595.

Galloway, D.L. *et al.* (1998). Detection of aquifer system compaction and land subsidence using interferometric synthetic aperture radar, Antelope Valley, Mojave Desert, California. *Water Resour. Res.* **34,** 2573-2585

Goovaerts, P. (1997). *Geostatistics for Natural Resources Evaluation.* Oxford University Press, Oxford

Hanssen, R.F. (2001). *Radar interferometry. Data Interpretation and Error Analysis* (Kluwer Academic Publisher, 2001)

Hernández-García, M.E. & Custodio, E. (2004). Natural baseline quality of Madrid tertiary detrital aquifer groundwater: a basis for aquifer management. *Environ. Geol.* **46,** 173-188

Hernández-Mora, N., Martínez, L., Llamas, M.R. & Custodio, E. (2007). Groundwater in the Southern Member States of the European Union: an assessment of current knowledge and future prospects. European Academies Science Advisory Council (EASAC), *Country report for Spain*. Available at:

http://www.easac.eu/fileadmin/PDF_s/reports_statements/Spain_Gro undwater_country_report.pdf (Date of access: 21st March 2016)

Hoffmann, J., Zebker, H., Galloway, D. & Amelung, F. (2001). Seasonal subsidence and rebound in Las Vegas Valley, Nevada, observed by synthetic aperture radar Interferometry. *Water Resour. Res.* **37,** 1551-1566

Hooper, A., Bekaert, D., Spaans, K. & Arikan, M. (2012). Recent advances in SAR interferometry time series analysis for measuring crustal deformation. *Tectonophysics* **514-517,** 1-13**;** DOI:10.1016/j.tecto.2011.10.013

Iglesias-Martín, J.A. *et al.* (2005). Modelo matemático de flujo del acuífero

terciario detrítico de Madrid explotado por el Canal de Isabel II. Paper presented at: *International workshop: from data gathering and groundwater modelling to integrated management, Alicante, Spain.* Madrid: Instituto Geológico y Minero de España. (2005, October) (in Spanish)

IGME. (2000). Geological Map of Spain, region 534. Technical report. (in Spanish). Available at:

http://info.igme.es/cartografiadigital/geologica/Magna50Hoja.aspx?Id=534#memoria_y_metadatos (Date of access: 21st March 2016).

IGME. (1989). Geological Map of Spain, region 559. Technical report. (in Spanish). Available at:

http://info.igme.es/cartografiadigital/geologica/Magna50Hoja.aspx?id=559#memoria_y_metadatos (Date of access: 21st March 2016).

Ireland,R.L.,Poland,J.F. & Riley, F.S. (1984). Land subsidence in the San Joaquin Valley, California, 1980, U.S. Geol. Surv.Prof. Pap., 437-I

Isaaks, E.H. & Srivastava, R.M. *An Introduction to Applied Geostatistics.* (Oxford University Press, 1989).

Jiao, J.J., Zhang, X. & Wang, X. (2015). Satellite-based estimates of groundwater depletion in the Badain Jaran Desert, China. *Sci. Rep.* **5,** DOI:10.1038/srep08960

Lanari, R. *et al.* (2004). A small baseline DIFSAR approach for investigating deformations on full resolution SAR interferograms. *IEEE Trans Geosci Remote Sens* **7,** 1377–1386

Llamas, R., Villarroya, F. & Hernández-García, M.E. (1996). Causes and effects of water restrictions in Madrid during the drought of 1990/93. Paper presented at Annual Meeting, American Institute of Hydrology: Hydrology and hydrogeology of urban and urbanizing areas, Boston. American Institute of Hydrology(1996, April).

Llamas, M.R. (2007). La Directiva Marco del Agua, remedio de hidroesquizofrenia. *Ilustración de Madrid* **6, 5-14** (in Spanish).

Llamas, M.R. & Garrido, A. (2007). Lessons from intensive groundwater use in Spain: economic and social benefits and conflicts. In "*The Agricultural Groundwater Revolution: Opportunities and Threats to Developmen*t, Giordano and Villholth (edits), CAB International, Wallingford, UK, 266-295

Martínez-Santos, P., Pedretti, D., Martínez-Alfaro, P.E., Conde, M., Casado, M. (2010). Modelling the Effects of groundwater-based urban supply in low-permeability aquifers: application to the Madrid Aquifer, Spain. *Water Resour. Manage.* **24,** 4613–4638

McGuire, V. *et al.* (2003). Water in Storage and Approaches to Ground-Water Management, High Plains Aquifer, 2000. *USGS Circular 1243*

Ministerio de Medio Ambiente. (2007). Plan especial de actuación en situaciones de alerta y eventual sequía de la cuenca hidrográfica del Tajo Anejo III - Análisis De Sequías Históricas *Technical report.* (in Spanish).

Available at:

http://www.chtajo.es/DemarcaTajo/SequiasyAvenidas/Documents/Memoria.pdf (Date of access: 21st March 2016).

Reeves, J.A., Knight, R. Zebker, H.A., Kitanidis, P.K. & Schreüder, W.A. (2014). Estimating temporal changes in hydraulic head using InSAR data in the San Luis Valley, Colorado. *Water Resour. Res.* **50,** 4459-4473; DOI:10.1002/2013WR014938

Remy, N., Boucher, A. & Wu, J. *Applied Geostatistics with SGeMS: A User's Guide.* (Cambridge University Press, 2009).

Richey, A.S. *et al*. (2015a). Quantifying Renewable Groundwater Stress with GRACE. *Water Resour. Res.* **51,** 5217-5238; DOI: 10.1002/2015WR017349

Richey, A.S. (2015b). *et al.* Uncertainty in Global Groundwater Storage

Estimates in a Total Groundwater Stress Framework. *Water Resour. Res.* **51,** 5198-5216; DOI:10.1002/2015WR017351

Riley, F.S. (1969). Analysis of borehole extensometer data from central California. Paper presented at: Tokyo Symposium: International Association of Hydrological Sciences (IAHS). Tokyo. IAHS publication 88, 423-431. (1969, September).

Riley, F.S. (1984). Developments in borehole extensometry. Paper presented at: International Symposium on Land Subsidence, 3rd, Venice. International Association of Scientific Hydrology Publication 151, 169– 186. (1984, March).

Rodríguez, J.M. (2000). Propiedades geotécnicas de los suelos de Madrid, vol. 3405. *Revista de Obras Públicas*, 59-84 (in Spanish).

Schmidt, D. A. & Burgmann, R. (2003). Time-dependent land uplift and subsidence in the Santa Clara valley, California, from a large interferometric synthetic aperture radar data set. *J. Geophys. Res.* **108,** 2416-2428; DOI: 10.1029/2002JB002267.

Shah, T., Molden, D., Sakthivadivel, R. & Seckler, D. (2000). The global groundwater situation: Overview of opportunities and challenges. *Colombo, Sri Lanka: International Water Management*
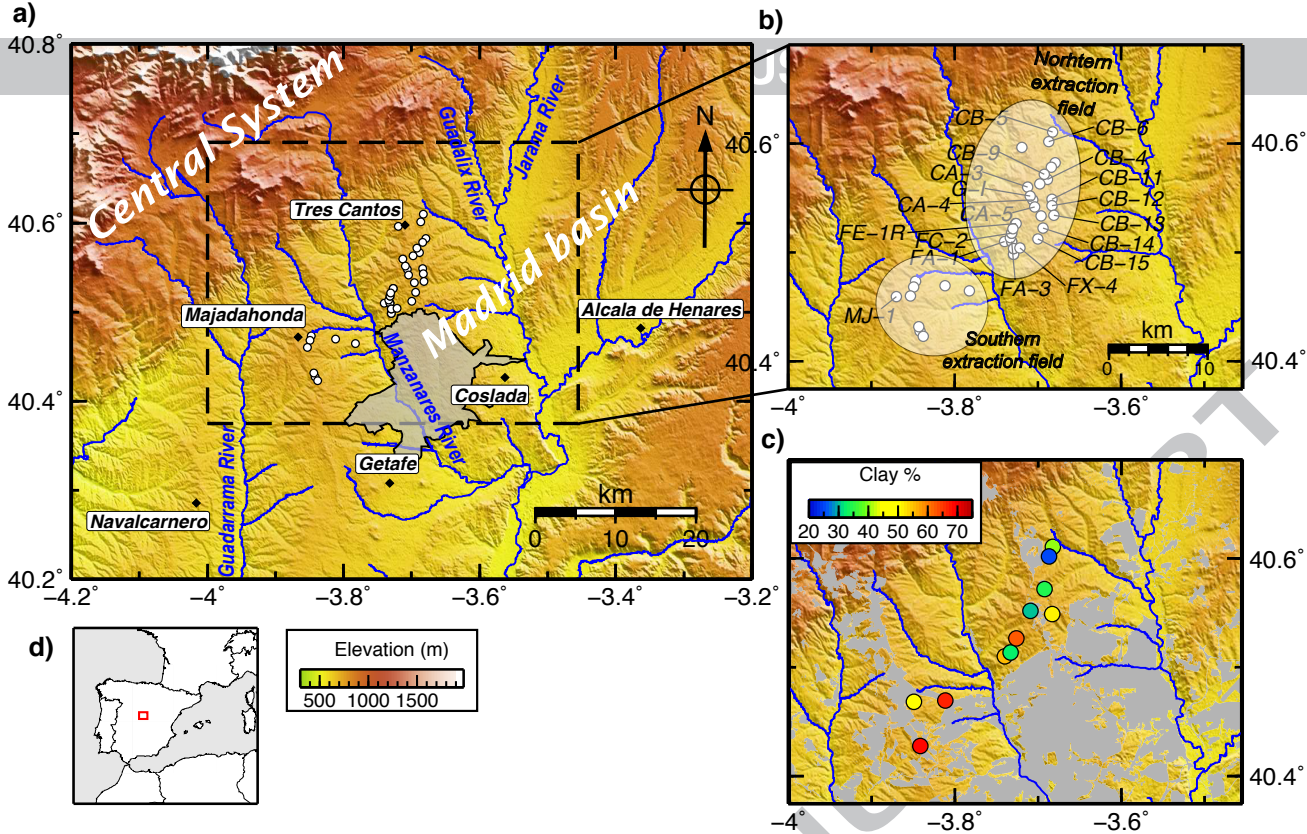
Available at:

http://publications.iwmi.org/pdf/H025885.pdf (Date of access: 21st March 2016).

Sneed, M. & Galloway, D.L. (2000). Aquifer-system compaction and land subsidence: measurements, analyses, and simulations: the Holly site, Edwards Air Force Base, Antelope Valley, California. *USGS Water-Resour Invest Rep 00-4015*. 65 pp. Available at: http://pubs.usgs.gov/wri/2000/wri004015/ (Date of access: 21st March 2016).

Tangdamrongsub, N. Ditmar, P.G., Steele-Dunne, S.C., Gunter, B.C. and Sutanudjaja, E.H. (2016). Assessing total water storage and identifying flood events over Tonlé Sap basin in Cambodia using GRACE and MODIS satellite observations combined with hydrological models. *Remote Sensing of Environment*, **181**, 162-173.

Todd, D.K. (1980). *Groundwater Hydrology*, 2nd edition (John Wiley & Sons, 1980).

Tomás, R. *et al.* (2009). A ground subsidence study based on DInSAR data: Calibration of soil parameters and subsidence prediction in Murcia City (Spain). *Eng. Geol.* **111,** 19–30.

Taylor, R. (2014). When wells run dry. *Nature* **516,** 179-180; DOI:10.1038/516179a.

Voss, K.A. *et al.* (2013). Groundwater depletion in the Middle East from GRACE with implications for transboundary water management in the Tigris-Euphrates-Western Iran región. *Wat. Resour. Res.* **49,** 904–914

Wada, Y. & Bierkens, M. F. P. (2014). Sustainability of global water use: past reconstruction and future projections. *Environ. Res. Lett.* **9**; DOI:10.1088/1748-9326/9/10/104003

WWF/Adena. (2006). Illegal water use in Spain. Causes, effects and solutions. *Technical report.*

Available at:

http://assets.panda.org/downloads/illegal_water_use_in_spain_may06.pdf. (Date of access: 21st March 2016).

Yélamos, J. G. & Villarroya, F. I. (1991). Variación de la piezometría y el caudal en cuatro explotaciones de aguas subterráneas en el acuífero del Terciario detrítico de Madrid. *Bol. Geol. Min.* **102,** 857-874 (in Spanish).

Yélamos, J.G. & Villarroya Gil, F. (2007). El acuífero terciario detrítico de

Madrid: pasado, posibilidades actuales y retos pendientes. *Enseñanzas de las Ciencias de la Tierra*, 317-324 (in Spanish)

Zektser, I. S. & Everett, L. G. (2004). Groundwater Resources of the World and Their Use. *UNESCO IHP-VI Series on Groundwater No 6.*
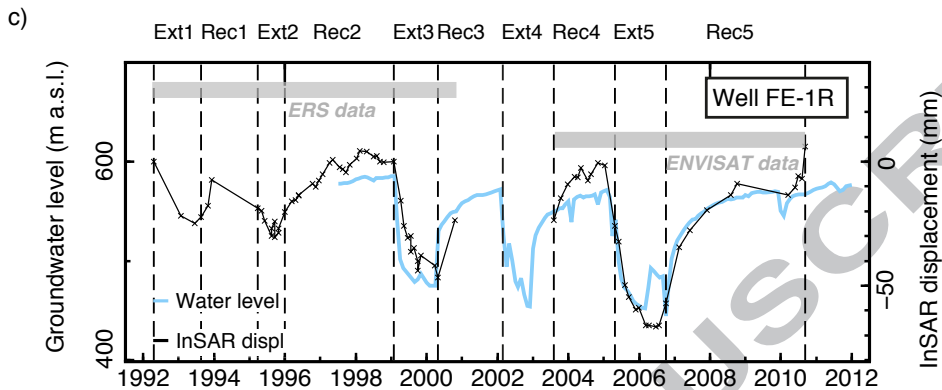
Available at:

http://unesdoc.unesco.org/images/0013/001344/134433e.pdf (Date of access: 21st March 2016).

Appendices

Appendix A. Estimation of elastic storage coefficient from stress displacement analysis.

Appendix B. Geostatistical analysis to interpolate groundwater level estimations in regions affected by decorrelation.

Supplementary data associated with this article can be found in the online version.
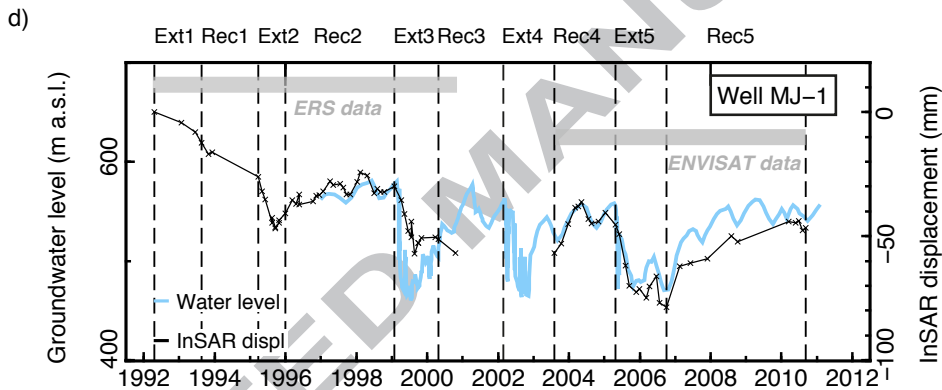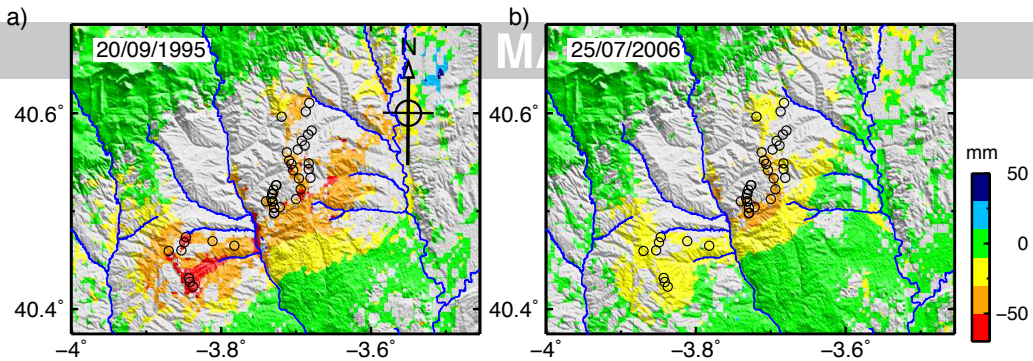
a) Map showing the Central System, Guadalix River, Jarama River, and Madrid basin with labeled locations: Tres Cantos, Majadahonda, Alcalá de Henares, Coslada, Getafe, Navalcarnero, Guadarrama River, Manzanares River.
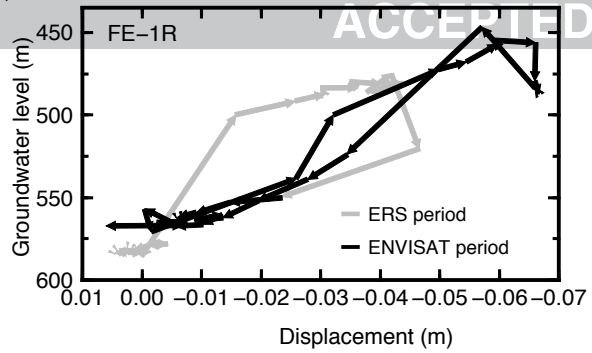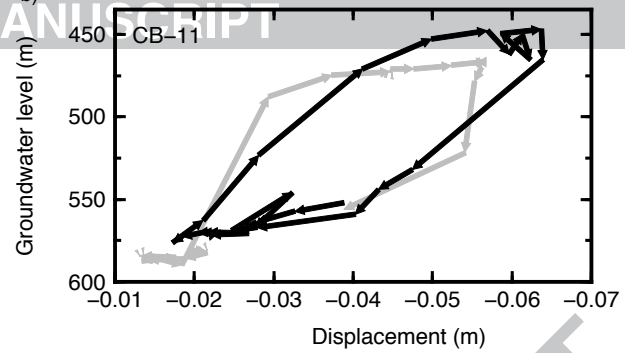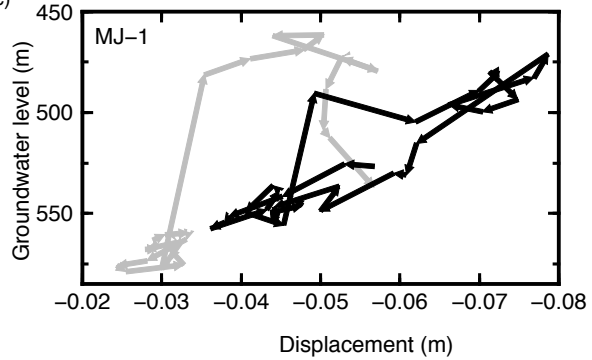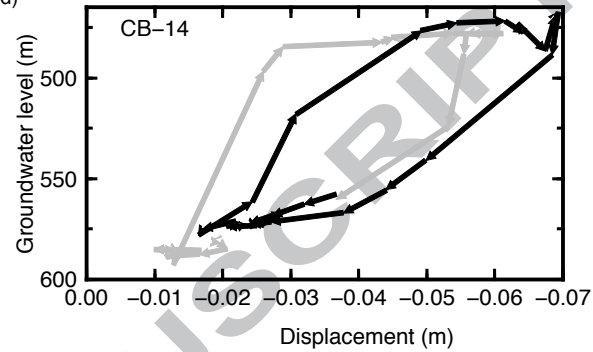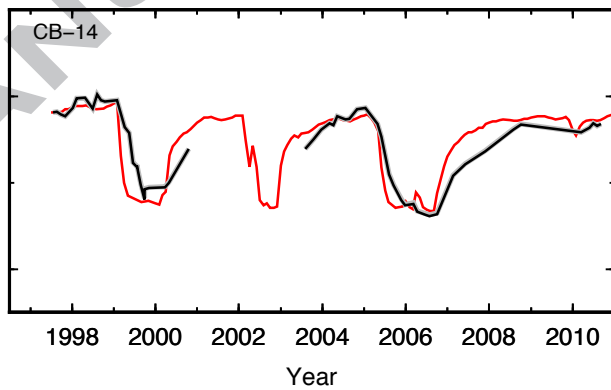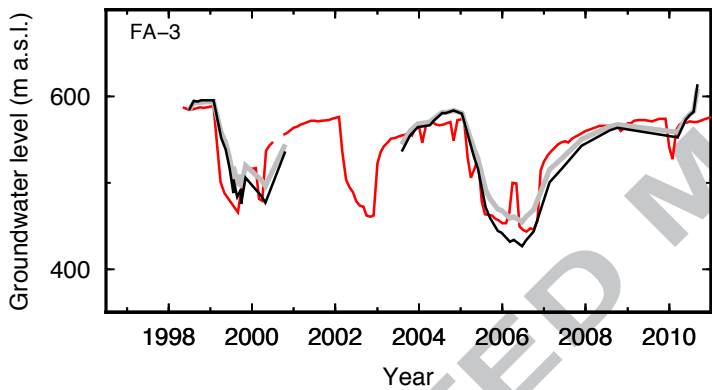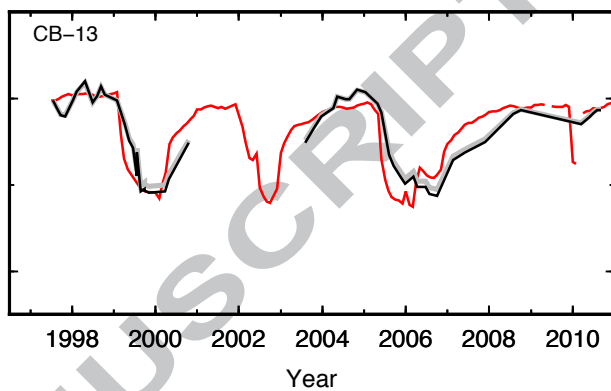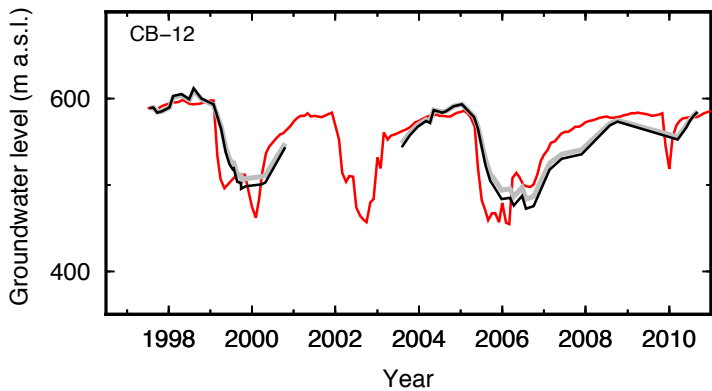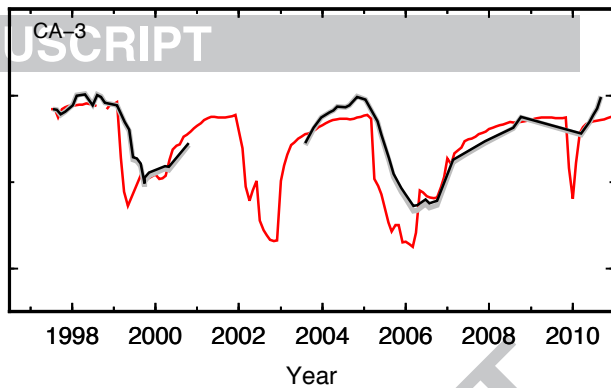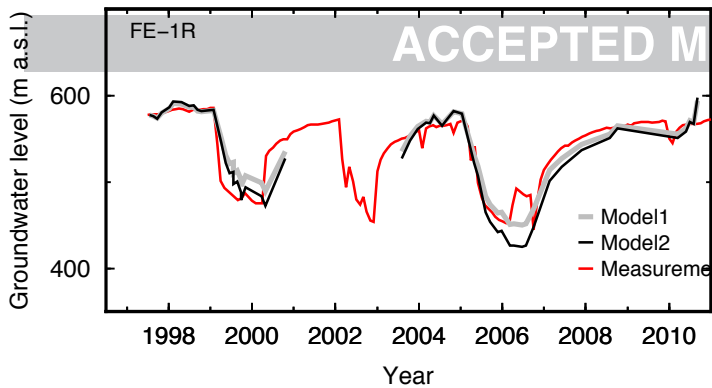
b) Detail map showing Northern extraction field and Southern extraction field with sample points: CB-5, CB-6, CB-9, CB-4, CA-3, CB-11, CA-1, CB-12, CA-5, CB-13, CA-4, CB-14, FE-1R, FC-2, CB-15, FA-1, FX-4, FA-3, MJ-1.

c) Map showing Clay % distribution with color scale (20, 30, 40, 50, 60, 70).

d) Location map of Spain with Elevation (m) scale (500, 1000, 1500).

a) V=-8.8 MCM

b) 19/APR/1992-27/JAN/1999

c) V=-4.9 MCM

d) 11/JAN/2005-07/SEP/2010

Volume (MCM): -0.02 0.00 0.02

InSAR displacement (mm): -40 -20 0 20 40
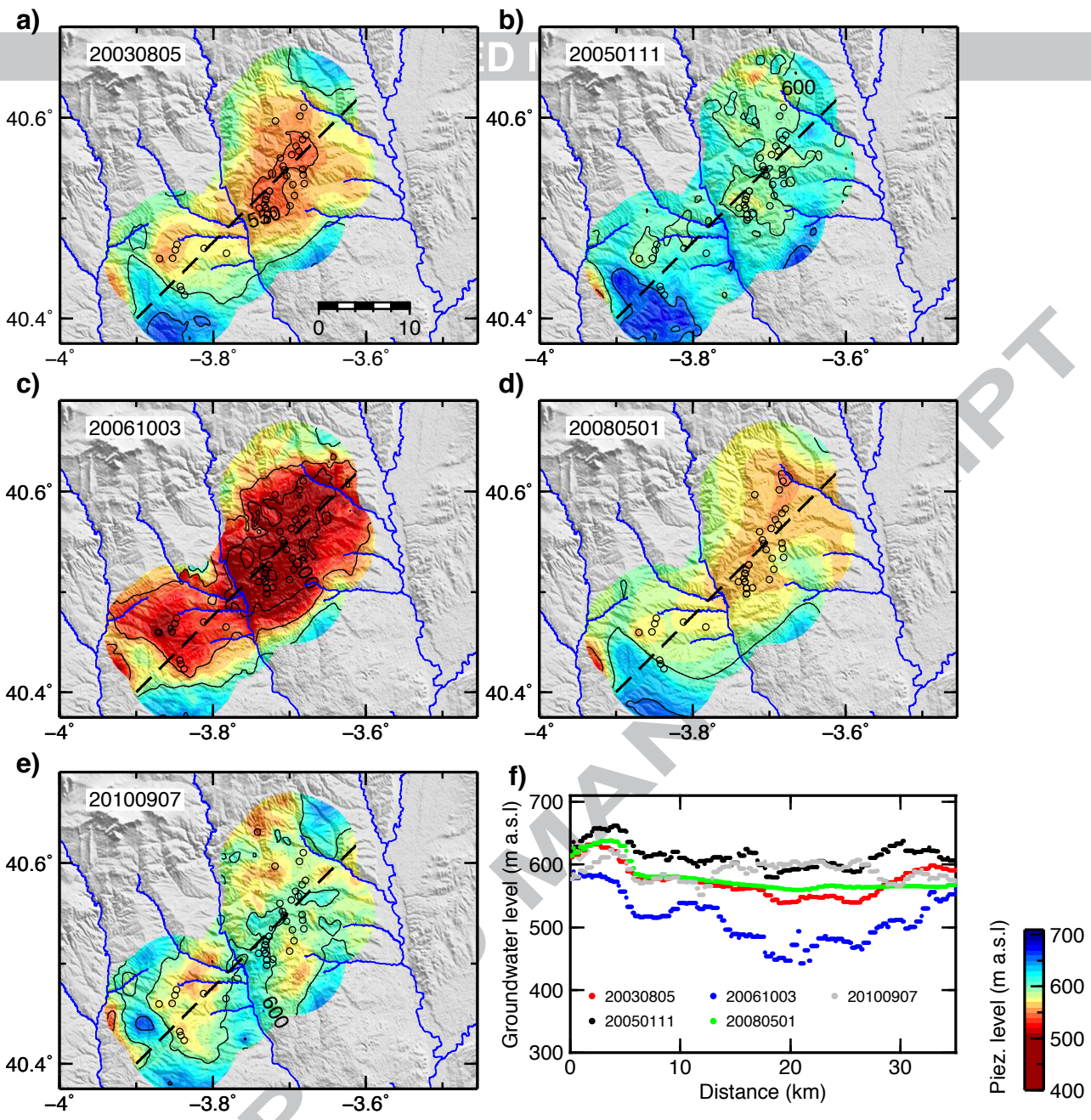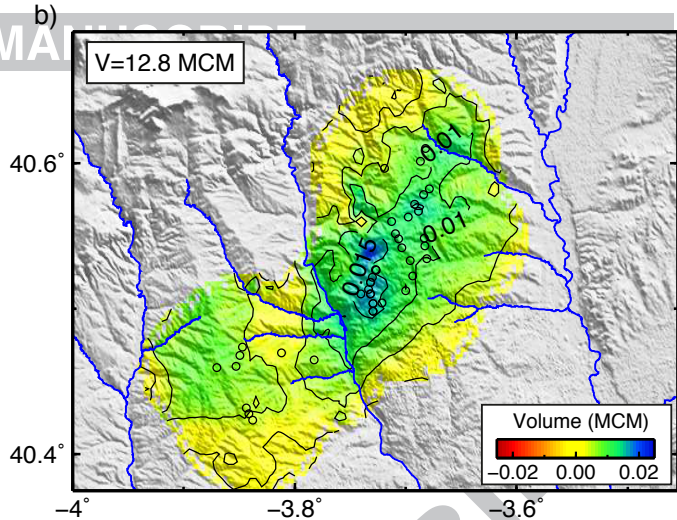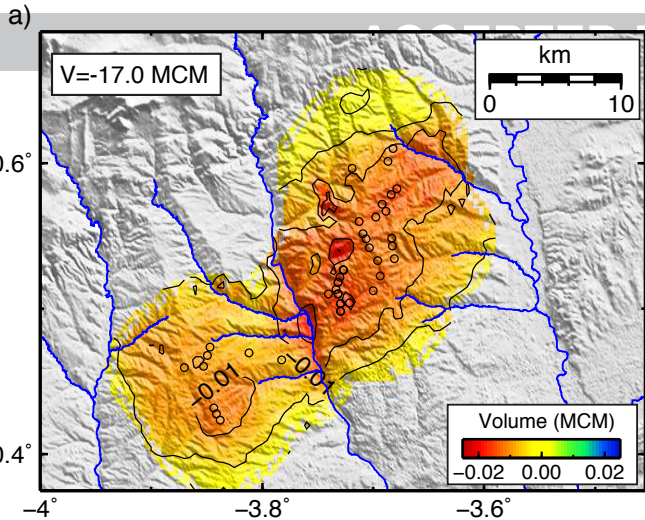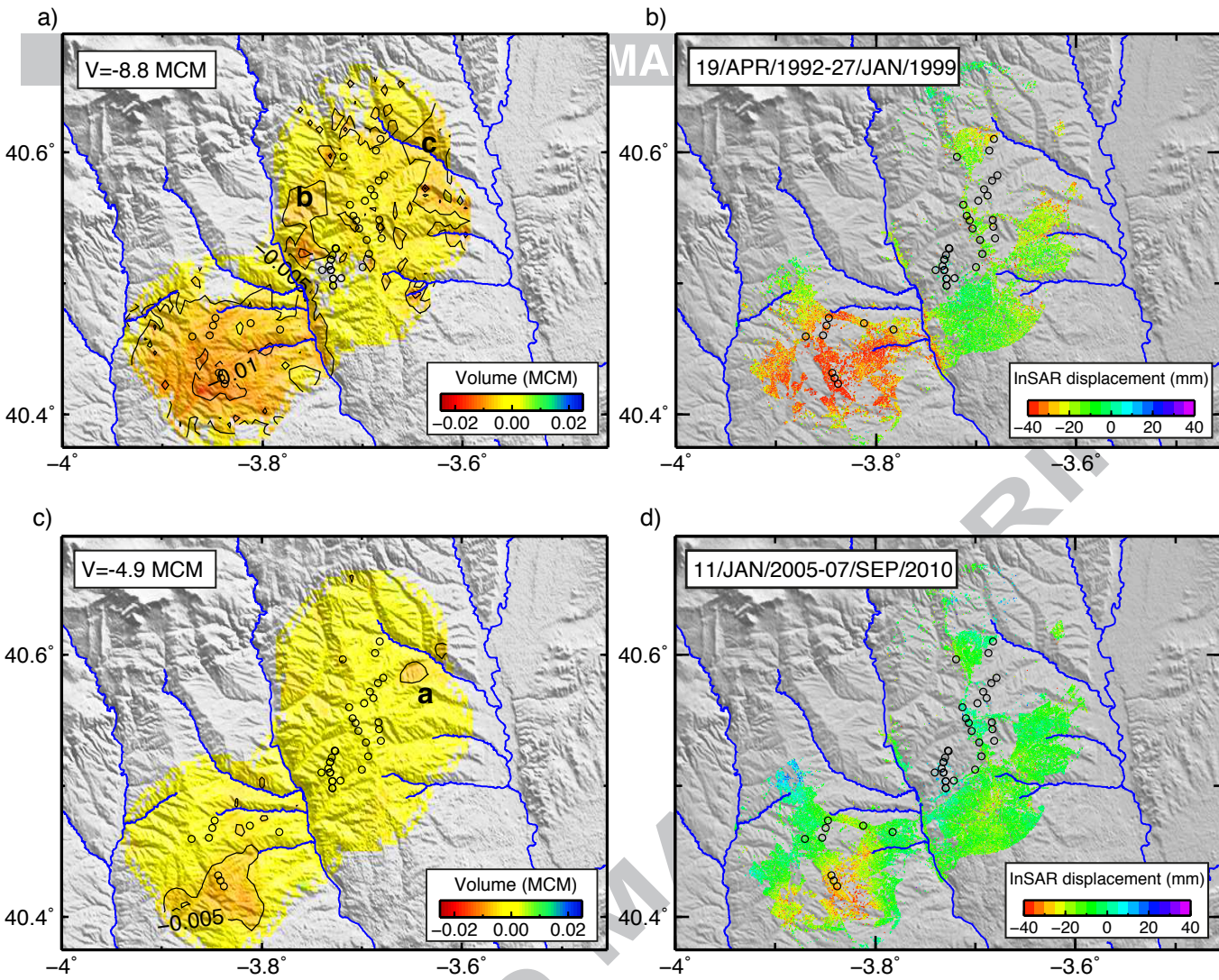
Mapping groundwater level and aquifer storage variations from InSAR measurements in the Madrid aquifer, Central Spain

Marta Béjar-Pizarro*[1,2,3], Pablo Ezquerro[1,3,5], Gerardo Herrera[1,2,3,4], Roberto Tomás[2,3,6], Carolina Guardiola-Albert[1,7], José M. Ruiz Hernández[8], José A. Fernández Merodo[1,2,3], Miguel Marchamalo[1,3,5], Rubén Martínez[3,5]

Highlights

- We map groundwater level and aquifer storage variations using satellite radar data.
- A combination of PSI and groundwater level data is used.
- The method helps to identify small aquifers affected by groundwater storage loss.